Lab on a Chip

Miniaturisation for chemistry, physics, biology, & bioengineering

www.rsc.org/loc

Volume 9 | Number 15 | 7 August 2009 | Pages 2105–2252

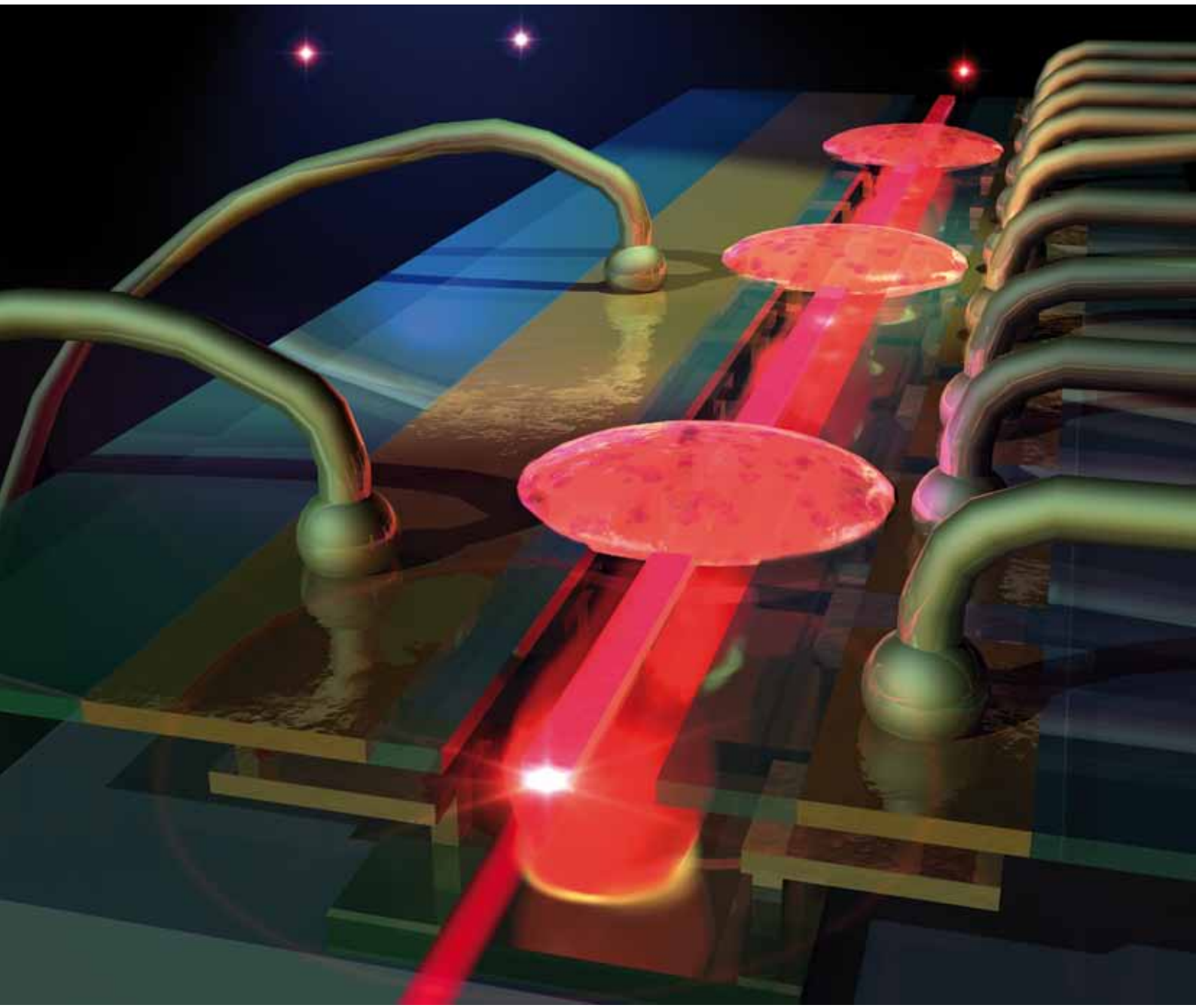

ISSN 1473-0197

RSC Publishing

1473-0197(2009)9:15;1-V

Label-free silicon photonic biosensor system with integrated detector array

Rongjin Yan,[a] Santano P. Mestas,[ab] Guangwei Yuan,[a] Rashid Safaisini,[a] David S. Dandy[bc] and Kevin L. Lear*[ab]

Received 3rd February 2009, Accepted 29th April 2009
First published as an Advance Article on the web 14th May 2009
DOI: 10.1039/b902111f

An integrated, inexpensive, label-free photonic waveguide biosensor system with multi-analyte capability has been implemented on a silicon photonics integrated circuit from a commercial CMOS line and tested with nanofilms. The local evanescent array coupled (LEAC) biosensor is based on a new physical phenomenon that is fundamentally different from the mechanisms of other evanescent field sensors. Increased local refractive index at the waveguide's upper surface due to the formation of a biological nanofilm causes local modulation of the evanescent field coupled into an array of photodetectors buried under the waveguide. The planar optical waveguide biosensor system exhibits sensitivity of 20%/nm photocurrent modulation in response to adsorbed bovine serum albumin (BSA) layers less than 3 nm thick. In addition to response to BSA, an experiment with patterned photoresist as well as beam propagation method simulations support the evanescent field shift principle. The sensing mechanism enables the integration of all optical and electronic components for a multi-analyte biosensor system on a chip.

1. Introduction

Refractive index (RI) sensing is one of the most important detection methods adopted for many label-free photonic biosensors, which have demonstrated high sensitivities in previous work.[1–8] However, limited by their detection principles, these traditional RI based sensors cannot detect the RI change locally, suffer from strong temperature dependence, and require sophisticated and expensive external components or instrumentation. These issues complicate integration of multi-analyte versions of these biosensors into a robust chip-scale system, and hence restrict their application. If appropriate biosensor technology could be reduced to a single integrated circuit platform, it would be extremely well suited for applications including the sensing of infectious disease biomarkers.[9] This paper discusses the design, fabrication and characterization of a novel biodetection chip that could serve as the basis for a multianalyte system with a volume of less than 1 cm^3.

The local evanescent array coupled (LEAC) biosensor concept is based on the physical phenomenon of local field redistribution when a waveguide cross-section changes in response to biofilm formation due to specific binding of molecules in localized regions. In related previous work, near field scanning microscopy (NSOM) was used to study the optical field respose to different films on a waveguide structure.[10,11] NSOM investigations on patterned C-reactive protein (CRP) immuno-complexes with immobilized anti-CRP antibody and multiple CRP concentrations show that the intensity modulation ratio sensitivity on a waveguide's top surface arising from a 1 nm change in thickness of a 15 nm nanofilm is approximately 1.7%/nm.[11]

For this work, rather than using bulky NSOM equipment, a photodetector array is integrated underneath a waveguide core to sense the vertical shift in the evanescent field due to patterned films. This is the first experimental demonstration of the LEAC biosensing system with integrated buried detectors. Use of asymmetric waveguides, potentially close to cutoff, and relatively large core to detector distances can provide very large normalized current modulation due to changes in surface film thickness. The multiple element detector array enables multianalyte biosensing on a single waveguide with multiple regions of various immobilized antibodies or other molecular recognition probes. A more complete description of the local evanescent field shift phenomenon including numerical simulations appears in the next section.

Conventional optical waveguide or fiber sensors such as surface plasmon resonance (SPR) devices[1–4] rely on an evanescent field interaction with the bound layer to alter the amplitude, phase, or angle of the transmitted light after it has left the immobilized probe region. The associated systems typically convert all of the transmitted light with a single detector allowing only one detector and thus one analyte per waveguide or optical path. In contrast, the local field shift mechanism permits the LEAC sensor to detect the index change in or near each different molecular probe region. Multiple probe regions with intervening reference regions without specific binding, all placed sequentially along the waveguide, allow simultaneous sensing of multiple analytes using the structure illustrated in Fig. 1. Simultaneous sensing on a single waveguide along with integrated, on-chip detectors, enables the LEAC biosensor structure to be much more compact than alternative photonic immunosensor approaches.

High-Q ring and disk[5–7] resonator biosensors can provide extremely low limits of detection, for example sensing single molecule binding. However, their high Q also makes them very

[a]*Department of Electrical and Computer Engineering, Colorado State University, Fort Collins, Colorado, 80523-1373, USA. E-mail: Kevin.Lear@colostate.edu; yanrj@engr.colostate.edu; Tel: +970-491-0718*
[b]*School of Biomedical Engineering, Colorado State University, Fort Collins, Colorado, 80523-1376, USA*
[c]*Department of Chemical and Biological Engineering, Colorado State University, Fort Collins, Colorado, 80523-1370, USA*

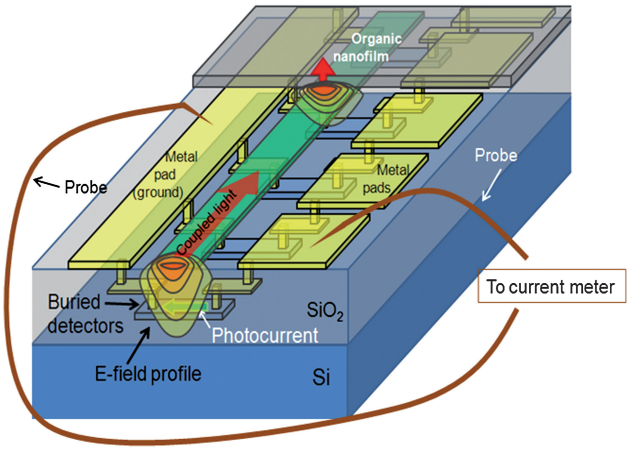

Fig. 1 Schematic diagram of a LEAC biosensor CMOS chip where evanescent field distribution shifts up upon reaching the organic nanofilm, resulting in decreased photocurrent in detectors under the film.

sensitive to temperature changes. This temperature sensitivity is an attribute shared by other sensors based on resonances, including SPR, and necessitates separate reference sensors to compensate for temperature changes. The very narrow line widths of high-Q resonators also require the incorporation of high resolution spectrometers or tunable laser sources to monitor resonant wavelength shifts. The LEAC biosensor is a non-resonant device with a minimal temperature sensitivity for the modulation ratio of $-0.3\% \pm 0.15\%/\,^{\circ}C$.[12] Further, the LEAC biosensor can operate with LEDs, which offer both noise and system simplification advantages.

The remainder of this paper describes the underlying mechanism of evanescent field shift with the support of numerical simulations in Section 2 and then presents experimental confirmation in Section 3 using deposited films on the first waveguide samples containing integrated detector arrays under the waveguides.

2. Simulation

As shown in Fig. 1, nanoscale organic layers, such as those formed by the binding of target antigens or antibodies, increases the effective refractive index just above the silicon nitride waveguide core and hence shifts the evanescent field profile away from the underlying buried detectors, reducing the associated photocurrent. An asymmetric waveguide structure amplifies the modulation of light intensity below the waveguide where the buried detector array is placed. Beam propagation method (BPM) simulations were used to study the electromagnetic field distribution of guided light in a ridge waveguide structure when organic films of different thicknesses were patterned on the waveguide surface. In Fig. 2(a), a logarithmic plot of the electric field profiles for film thicknesses from 0 to 40 nm shows that thicker films make small normalized changes in the field strength near the core but very large relative changes at large distances from the core. The slope of the E-field plots in the cladding are proportional to the evanescent decay constant, γ. The simulated dependence of the decay constant on film thickness, d, appears in Fig. 2(b). Since the light intensity decays exponentially in the lower cladding, positioning a detector further from the waveguide core can increase its light intensity modulation ratio,

$$\frac{\Delta I}{I_0} \approx \frac{\exp(-2\gamma_{\text{film}}s) - \exp(-2\gamma_0 s)}{\exp(-2\gamma_0 s)} = \exp\left(-2(\gamma_{\text{film}} - \gamma_0)s\right) - 1 \quad (1)$$

at a distance s below the waveguide core in response to the adsorption of a film on the surface that shifts the evanescent field decay constant from γ_0 to γ_{film}. The normalized photocurrent modulation of a thin linear detector will be approximately the same as the intensity modulation ratio. The evanescent decay constant varies along the waveguide according to the local film thickness in that region, so that a photodetector array can sense varying organic film thicknesses such as those that would result from different levels of specific binding along the waveguide if it were patterned with different probe molecules in different regions.

As presented below, sensing with an integrated photodetector array $s = 1.5$ μm below the waveguide core results in a light intensity modulation ratio of approximately 20% upon a 1 nm change in thickness, which is about 10 times larger than the NSOM measured result (1.7%/nm) on the waveguide surface,[11] and eliminates the need for large instrumentation. Thus, the integrated photodetector array configuration of the LEAC sensor demonstrates greater sensitivity and enables system miniaturization which lends to the potential of an ambulatory or point-of-care device.

BPM simulations were used to investigate the light intensity modulation ratios in response to the addition of surface films of varying thicknesses for different potential detector positions above and below the waveguide core. The modulation ratios due to the change in intensity from the case with no film to a film up to 100 nm thick are shown in Fig. 2(c). For a biofilm thickness of 2.5 nm, the light intensity modulation on the waveguide and film surface, approximating the case of NSOM measurements, is expected to be +5%, while the modulation ratio 1.5 μm under the waveguide, corresponding to a buried photodetector, is predicted to be −30%. These simulations predict that much larger modulation ratios can be obtained using buried detector arrays, and this trend is confirmed by the following experimental results. While the sensor's non-linear response to organic film thickness would slightly complicate calibration, which can easily be implemented with future on-chip electronics, the approximately logarithmic behavior simultaneously offers a lower limit of detection and larger dynamic range.

According to eqn (1), positioning the buried detector farther from the waveguide core structure, *i.e.* increasing s, provides a larger modulation ratio and hence higher sensitivity. Analysis of the simulation data quantifies the relationship between the modulation ratio sensitivity and the detector's position and is presented in Fig. 2(d). For moderately thick organic layers, the sensivity changes little at different detector positions since the modulation ratios have saturated in these cases. However, when the organic films are thinner there is a strong dependence on detector depth. For example, for a subnanometer layer of $d = 0.2$ nm, the sensitivity increases from 6.4%/nm at 0.5 μm below the waveguide to 21%/nm at 2 μm, which indicates deeper detector postions offer a significantly increased sensitivity when the LEAC sensor is used to detect nano-scale

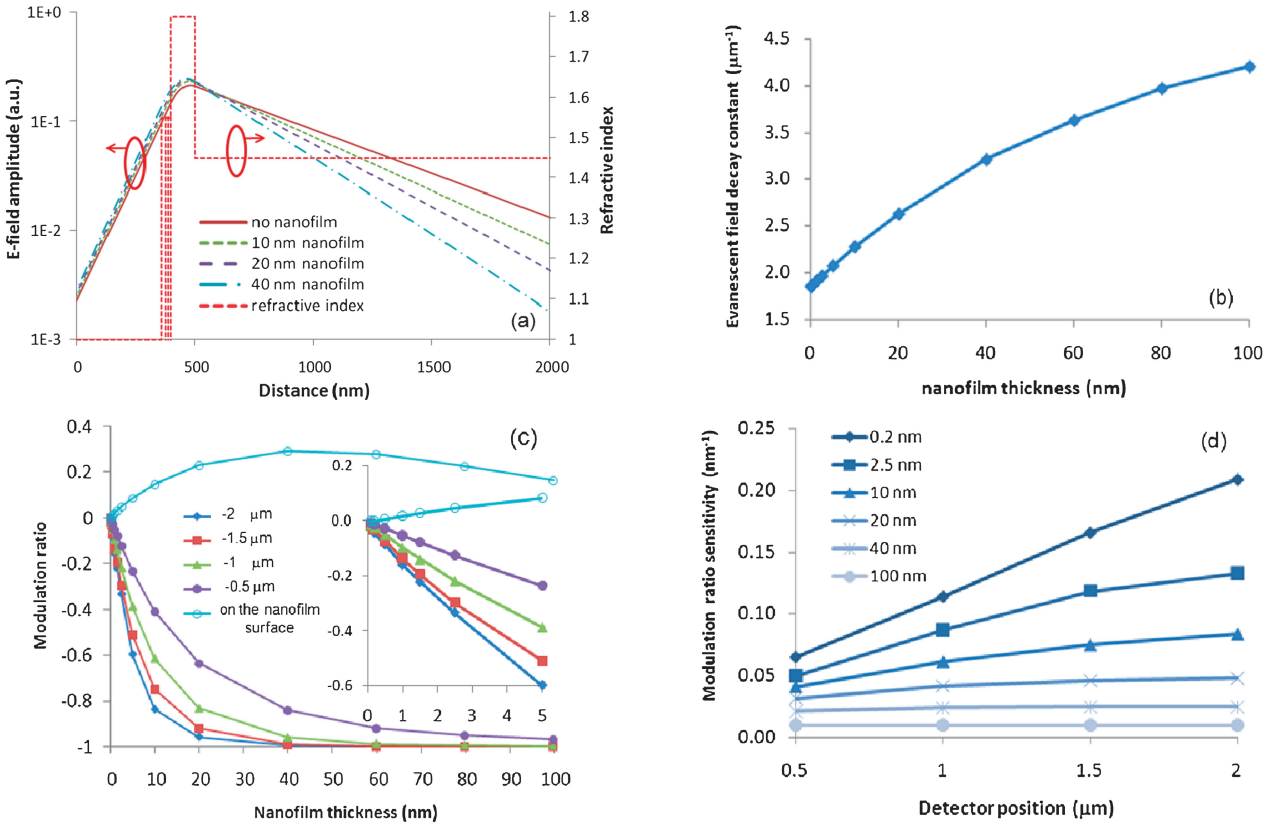

Fig. 2 (a) E-field decays exponentially as a function of depth into the lower waveguide cladding at different rates depending on nanofilm thickness (0–40 nm). The refractive index profile of the waveguide structure is shown (dotted lines) with air as the upper cladding, SiN_x as the waveguide core, and SiO_2 as the lower cladding. (b) Evanescent field decay constant dependence on nanofilm thickness. (c) Simulated modulation ratio as a function of nanofilm thicknesses on the waveguide's top surface and for different vertical positions below the waveguide. (d) Sensitivity analysis of the LEAC sensor based on simulation data for different detector positions and film thicknesses.

biomolecules or biofilms. While moving the detector further from the waveguide core decreases the absolute magnitude of photocurrents, this trend could be counteracted by increasing guided mode power.

3. Experimental

3.1 Fabrication, sample preparation and data measurement

Fabrication of waveguide sensor chips with integrated detector arrays followed an abbreviated, two metal level, conventional commercial CMOS process flow similar to that described in ref. 13 except that MOSFETs were fabricated in the substrate and the SiN core waveguides were laterally defined by two etched trenches, as shown in Fig. 3(a), from the passivation layer placed on the top surface of the wafer. The core is separated from the 250 nm thick, undoped and unsilicided polysilicon photodetectors by a 1.5 μm SiO_2 layer, as seen in the SEM cross section. The buried detector array was connected to probe pads in metal-2 on the wafer surface by the metal-1 layer and two levels of vias. The lower vias served as contacts to the undoped polysilicon metal–semiconductor–metal photodetectors. In this work, 20 waveguide biosensing systems were implemented on a chip area of 20 mm^2, as shown in Fig. 3(b).

Waveguide end facets at the edges of individual die were polished for end-fire coupling of a 654 nm laser diode *via* visible single mode fiber (4/125 μm core/cladding diameter). A pair of probe needles applied a 1 V bias between each of the individual detector pads and the common ground pad, creating an electric field oriented perpendicular to the direction of light propagation for collecting photogenerated electrons and holes. The photocurrents were measured using either a HP4145 semiconductor parameter analyzer or a Keithley 2400 source meter. Fig. 1 shows the test configuration.

3.2 Photoresist film

To study sensor response to a patterned organic film, a 600 μm long, 120 nm thick photoresist layer ($n = 1.55$) was patterned across the waveguide above the 7th to 12th buried detectors, as shown in Fig 4(a). To obtain a thinned photoresist layer, AZ5214-E photoresist diluted in propylene glycol methyl ether acetate (PGMEA) was employed. An AZ5214-E : PGMEA (1 : 4) solution was spun on the sample at 6000 rpm for 30 s. The sample was then soft baked at 95 °C for 1 min to drive off the remaining solvent. Next, the photoresist layer was exposed with 10 mW/cm^2 405 nm UV light for 45 s after aligning a 600 μm width stripline photomask on the desired photodetectors. The sample was developed *via* immersion in AZ400K : H_2O (1 : 4) solution for 5

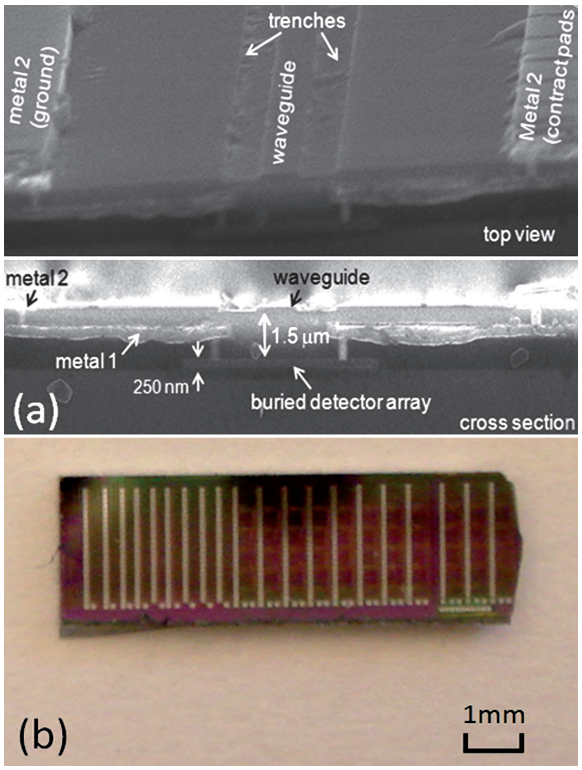

Fig. 3 (a) SEM images of the LEAC biosensor structure incorporating buried detectors. (b) 2.5 mm × 8 mm chip containing 20 biosensor systems consisting of waveguides with integrated detector arrays.

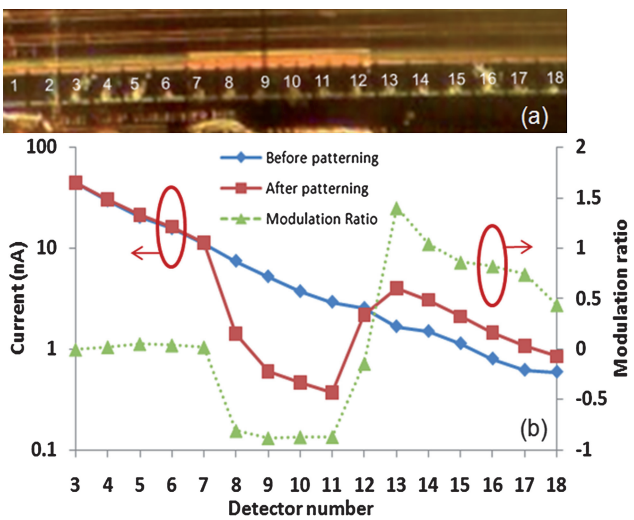

Fig. 4 (a) Photograph of a LEAC sensor waveguide with photoresist patterned above the 7th–12th detectors. (b) Photocurrents measured before (diamonds) and after (squares) the photoresist is patterned as well as the resulting modulation ratio (triangles).

to 10 s. Post baking the sample at 100 °C for 1 min hardened the photoresist after developing. NSOM topographic analysis shows a 120 nm thick photoresist on the 7th to 12th photodetectors.

Measured photocurrents from detector array elements before photoresist coating, plotted with diamonds in Fig. 4(b), are proportional to the light in the guided mode and exponentially decrease along the waveguide as the power in the waveguide is attenuated. After patterning the photoresist, the photocurrents shifted to the values indicated by the squares, dropping significantly in most of the photoresist region and returning to near the original value afterwards.

The modulation ratio for each detector is shown with triangles in Fig. 4(b). The ratio decreases from approximately zero to −0.87, *i.e.* the photocurrent decreases by 87%, due to the patterned photoresist film. The modulation ratio rises back to +1.4 at the 13th detector. These results imply that the light field is shifted up at the waveguide location where there is photoresist, and hence the photocurrent in the buried detectors under the waveguide decreases at that location. The photocurrents beyond the photoresist are higher than the original values due to reduced absorption by the photodetectors under the photoresist, leaving more power in the guided mode.

Due to light scattering by the edge of the relatively thick 120 nm photoresist film, the photocurrents collected by the 7th and 12th photodetectors are higher than the other photodetectors in the photoresist covered region, which leads to the minimal modulation ratios on these two detectors. The positive modulation ratio after the 12th detector means that the photocurrent returns to higher levels beyond the photoresist, and this indicates the large current decrease for the 8th to 11th detector is not caused by greatly reduced power in the waveguide as might be suspected in the case of extreme scattering.

As observed on the photoresist sample, each sensing region can modulate the subsequent guided mode power producing a minor complication for multiple analyte measurements. If multiple sensing regions are patterned on the same waveguide, changes in the guided power due to regions closer to the optical source would alter the power incident on subsequent sensing regions and thus the photocurrent detected in the latter regions. However, this cause of potential interference or cross-talk between regions can be remedied by incorporating blank or blocked reference regions and detectors prior to each sensing region. A differential measurement of the reference photocurrent relative to the immediately subsequent sensing region photocurrent would then allow for accurate determination of the local modulation ratio.

3.3 BSA film

To examine the response of the sensor to thinner organic nanofilms that are comparable to the thicknesses expected for immuno-complexes, BSA was patterned on the waveguide of another chip above 9 photodetectors (6th through 14th), as shown in Fig. 5(a). The BSA was labeled with fluorescein isothiocyanate (FITC), obtained from Sigma, according to the manufacturer's protocol. Phosphate buffered saline (PBS) solution was comprised of 50 mM sodium phosphate, 150 mM sodium chloride, 0.05% Tween 20, in deionized water and adjusted to pH 7.4. FITC-BSA patterning was achieved by manual delivery of 1 mg/mL FITC-BSA in PBS solution using a customized polypropylene–polyethylene copolymer based microcapillary device. Once delivered to the die surface, the FITC-BSA solution was incubated for 20 min at room temperature in a humidity controlled chamber. Following incubation, the die was rinsed with PBS, then deionized water, and dried

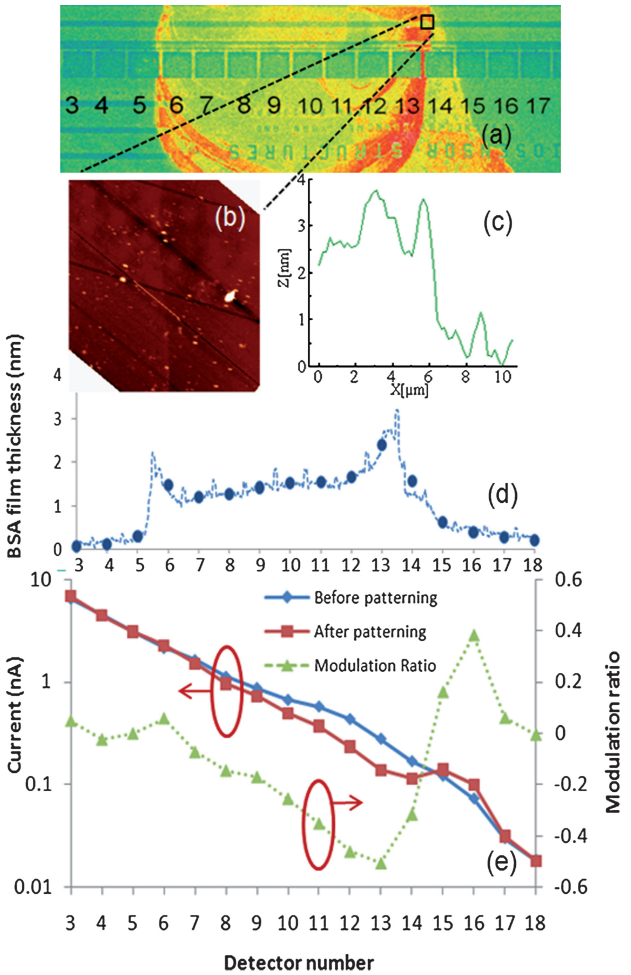

Fig. 5 (a) Fluorescence microscope image of a LEAC sensor waveguide with BSA patterned above the 6th–14th detectors. (b) False intensity AFM topographic image at the indicated position containing the edge of the BSA pattern. (c) Average nanofilm height obtained from AFM data. (d) BSA film thickness along the waveguide (dotted line) and average BSA film thickness above each photodetector (solid circle). (e) Photocurrents measured before (diamonds) and after (squares) the BSA is patterned as well as the photocurrent ratio (triangles).

under nitrogen. BSA was fluorescently labeled with FITC to enhance visualization of the pattern, as shown in Fig. 5(a), and to quantify the relative amount of adsorbed BSA, but fluorescent labeling is not required for the LEAC sensor mechanism.

Atomic force microscopy (AFM) was used to scan a 50 × 50 μm square area of the sample indicated in Fig. 5(a), to quantify the BSA film thickness. The scanned area was chosen to include the thickest edge of the BSA pattern as determined from the fluorescence image. The topography is shown in Fig. 5(b) and demonstrates that the average thickness of the BSA pattern on the left side of the scanned area is 2.5 nm, as shown by column average plotted in Fig. 5(c). Assuming that the average thickness of the BSA film is proportional to the fluorescent intensity, the 2.5 nm step height from AFM was used to calibrate the average thickness of the BSA film above each photodetector, and the result indicates it varies from 1.2 nm to 2.5 nm, as shown in Fig. 5(d).

As was observed in the photoresist experiment, the modulation ratios at the first and last detector under the BSA nanofilm were affected by light scattering. However, the modulation ratio of approximately −50% at the penultimate detector, #13, where the BSA film thickness was estimated to be 2.5 nm, is larger than the BPM simulated modulation ratio of −30%. In this experiment, the LEAC biosensor system shows a sensitivity of approximately 20%/nm when the patterned nanofilm is 2.5 nm.

4. Conclusion

A novel type of optical waveguide biosensor system was designed, fabricated and tested using organic nanofilms. The sensing mechanism is based on the physical phenomenon of local evanescent field redistribution coupled to an integrated detector array buried beneath the waveguide. The redistribution phenomenon is comfirmed by numerical simulations and measured photocurrent modulation. Furthermore, the system was implemented on a chip *via* trailing-edge, low-cost commercial CMOS technology. The biosensor system was found to exhibit sensitivity of 20% modulation per nm in response to the addition of nanofilms to the surface of the waveguide.

This technology also may prove to have many advantageous features in terms of future development. As the system is based on a multiple element detector array, it is capable of simultaneously sensing multiple analytes. This multi-analyte capability, coupled with simulated and measured data supporting potential for high sensitivity, low temperature dependence, and independence from sophisticated external optical instrumentation supports the hypothesis that this system could be employed as a field portable device for many biosensing applications.

Acknowledgements

This project was supported in part by National Institutes of Health Grant No. EB00726. Additional support for SPM was provided by the National Science Foundation Bridge to Doctorate Fellowship. The authors acknowledge Avago Technologies Company for sensor fabrication. We also greatly thank Charles Thangaraj and Dr. Tom Chen in the Department of Electrical and Computer Engineering and Justin Sambur, Dr. Bruce Parkinson, Brian Murphy and Dr. Charles S. Henry in the Department of Chemistry, Colorado State University, for technical assistance, resource sharing and helpful discussions.

References

1 M. Malmqvist, *Nature*, 1993, **361**, 186–187.
2 Y. Luo, F. Yu and R. N. Zare, *Lab on a Chip*, 2008, **8**, 694–700.
3 R. D. Harris and J. S. Wilkinson, *Sensors and Actuators B: Chemical*, 1995, **29**, 261–267.
4 J. Rooney and E. Hall, *Sensors and Actuators B: Chemical*, 2006, **114**, 804–811.
5 K. De Vos, I. Bartolozzi, E. Schacht, P. Bienstman and R. Baets, *Optics Express*, 2007, **15**(7615), 7610.
6 M. Sumetsky, R. Windeler, Y. Dulashko and X. Fan, *Optics Express*, 2007, **15**(14381), 14376.
7 N. M. Hanumegowda, C. J. Stica, B. C. Patel, I. White and X. Fan, *Applied Physics Letters*, 2005, **87**, 201107–3.
8 M. Lee and P. Fauchet, *Optics Express*, 2007, **15**, 4530.
9 M. J. Sartain, R. A. Slayden, K. K. Singh, S. Laal and J. T. Belisle, *Mol. Cell Proteomics*, 2006, **5**, 2102–2113.

10 R. Yan, G. Yuan, S. Mestas, R. Safaisini and K. L. Lear, *21st Annual Meeting of the IEEE Lasers and Electro-Optics Society*, 2008, 240–241.
11 R. Yan, G. Yuan, M. D. Stephens, X. He, C. S. Henry, D. S. Dandy and K. L. Lear, *Applied Physics Letters*, 2008, **93**, 101110–3.
12 R. J. Yan, S. P. Mestas, G. Yuan, R. Safaisini and K. L. Lear, *IEEE Journal of Selected Topics in Quantum Electronics*, 2009, DOI: 10.1109/JSTQE.2009.2017207, , in press.
13 R. Pownall, Guangwei Yuan, T. Chen, P. Nikkel and K. Lear, *Photonics Technology Letters*, 2007, **19**, 513–515.

